[Cancer Biology & Therapy 7:7, 1006-1013; July 2008]; ©2008 Landes Bioscience

Research Paper

Contrast enhanced MRI and intravital fluorescence microscopy indicate improved tumor microcirculation in highly vascularized melanomas upon short-term anti-VEGFR treatment

M.E. Eichhorn,[1,2,*] S. Strieth,[2,3] S. Luedemann,[2] A. Kleespies,[1] U. Nöth,[4] A. Passon,[2] G. Brix,[5] K.W. Jauch,[1] C.J. Bruns[1] and M. Dellian[2,3]

[1]Department of Surgery; [2]Institute for Surgical Research; [3]Department of Otorhinolaryngology; Klinikum Grosshadern; University of Munich (LMU); Germany; [4]Institute of Radiation Biology; Helmholtz Center Munich—German Research Center for Environmental Health; Neuherberg, Germany; [5]Department of Medical Radiation Hygiene; Federal Office for Radiation Protection; Neuherberg, Germany

Key words: angiogenesis, anti-angiogenic tumor therapy, MRI, normalization, VEGF, SU5416

Anti-angiogenic therapy by blocking VEGF signalling combined with standard chemotherapy is a novel strategy for clinical cancer treatment. The mechanisms for enhanced antitumoral effects are still a matter of controversial debate. Tumor vessel "normalization" upon anti-angiogenic therapy leading to improved drug delivery has been proposed as possible mechanism. Therefore, aim of the study was to investigate tumor microvascular function upon anti-VEGFR treatment in highly vascularized melanomas. A detailed intravital-microscopic analysis of tumor microcirculation including the distribution pattern of vessel diameters and blood flow velocities was performed in melanomas grown in dorsal skinfold chambers of hamsters. Animals with highly vascularized established tumors were treated by a VEGFR tyrosin kinase inhibitor (SU5416) on three repetitive days. Tumor tissue oxygenation was measured by phosphorescence quenching technique. Overall tumor microcirculation of subcutaneous tumors was investigated by contrast enhanced MRI (CE-MRI). Vessel density was significantly decreased in treated animals. A significant shift in the distribution patterns towards increased vessel diameters and faster red blood cell velocities in remaining tumor vessels was observed upon anti-VEGF treatment, compensating reduced vascular density. Moreover, a trend towards elevated pO_2 levels in treated tumors was observed. Compared to controls, inflow kinetics of tumors quantified by CE-MRI as well as overall uptake of contrast agent in tumor tissue were significantly increased following short-term SU5416 treatment. In conclusion the results confirm temporarily improved tumor microvascular function in highly vascularized melanomas upon short term anti-VEGFR treatment leading to enhanced tumor blood supply and oxygenation potentially improving the efficacy of simultaneous chemo- or radiotherapy.

*Correspondence to: M.E. Eichhorn; Department of Surgery; Klinikum Grosshadern; University of Munich; Marchioninistrasse 15; Munich 81377 Germany; Tel.: +4989.7095.0; Fax: +4989.2443.40591; Email: martin.eichhorn@med.uni-muenchen.de

Submitted: 01/25/08; Revised: 03/23/08; Accepted: 03/29/08

Previously published online as a *Cancer Biology & Therapy* E-publication: http://www.landesbioscience.com/journals/cbt/article/5997

Introduction

Angiogenesis, the formation of new blood vessels from the endothelium of the existing vasculature, is fundamental in tumor growth, progression and metastasis.[1,2] Following the discovery and isolation of pro- and anti-angiogenic factors and preclinical development of anti-angiogenic drugs, there has been both enthusiasm and disappointment concerning the clinical efficacy of anti-angiogenic therapy during the past decade. Despite numerous promising results in preclinical investigations, initially no convincing clinical trial gave evidence for efficient antitumoral therapy yielding long term survival benefits by classical anti-angiogenic agents as monotherapy. Transferring results from preclinical animal models, it was a widely held belief that anti-angiogenic therapy also in human tumors eradicates tumor vasculature, thus depriving the tumor of oxygen and nutrients necessary for survival and tumor growth. In 2001, Rakesh K. Jain was the first to hypothesize "normalization" of tumor vasculature in response to anti-angiogenic therapy to be a possible complementary mode of action of anti-angiogenic drugs.[3-7] The hypothesis was driven by experimental data indicating improved antitumoral efficacy of radiation and chemotherapy when combined with anti-angiogenic therapy.[8-11] This observation was paradoxical, as the efficacy of radiation and chemotherapy depend on tumor blood supply and tissue oxygenation, respectively, which was expected to be impaired by anti-angiogenic therapy. Therefore, Jain proposed that immature and inefficient angiogenic tumor blood vessels could be pruned resulting in a more "normal" and more conductive tumor microcirculation for delivery of oxygen, nutrients and therapeutics.[3,4]

In contrast to an enormous number of preclinical studies investigating novel developed anti-angiogenic compounds in terms of antitumoral efficacy only a few number of investigation focus on functional changes of tumor microcirculation[12-14] in particular if already established highly vascularized tumors are treated by anti-angiogenic drugs. Yet, experimental results proving the hypothesis of "normalizing" tumor vasculature are limited to a rather small number of different experimental tumor models, few anti-angiogenic

©2008 LANDES BIOSCIENCE. DO NOT DISTRIBUTE.

compounds, mainly the VEGFR2 antibody DC101, and a limited number of treatment schedules. Moreover, to further optimize scheduling of anti-angiogenic therapy in combination with chemo- or radiotherapy, non-invasive imaging techniques are highly desired to monitor functional changes of tumor microcirculation.

In this context, aim of the present study was to investigate functional changes of tumor microcirculation in highly vascularized, established tumors in response to short term anti-angiogenic treatment. We investigated tumor microcirculation of subcutaneous A-MEL-3 melanomas non-invasively by contrast enhanced magnetic resonance imaging (CE-MRI) in response to anti-angiogenic treatment by the VEGFR tyrosine kinase inhibitor SU5416. In addition, initial morphological and functional changes of tumor microcirculation as well as tumor tissue oxygenation were analyzed by intravital microscopy and phosphorescence quenching technique, respectively.

Results

Subcutaneous tumor growth. Exponential tumor growth was observed in all tumors of control animals (Fig. 1). After two days of anti-angiogenic treatment, tumor growth in SU5416 treated animals was significantly delayed compared to controls. On day eight tumor volume in control animals was 1016 ± 173 mm^3, whereas tumor volume in SU5416 was effectively reduced to 335 ± 24 mm^3.

Tumor microcirculation investigated by CE-MRI. Concentration-time data of Gd-DTPA in arterial blood and tumor tissue are given in Figure 2A and B, respectively. Immediately after start of intravenous contrast agent infusion, a linear increase of contrast agent concentration was registered in arterial blood and tumor tissue. Both the slope of arterial input function and maximal peak enhancement in arterial blood was similar in both groups due to the standardized infusion of contrast agent and almost identical cardiac outputs in animals of both groups (Fig. 2A). In contrast, to arterial input functions, concentration-time data in tumor tissue clearly revealed different shapes as depicted in Figure 2B. Analysis of initial uptake kinetics in tumor tissue using linear regression (Fig. 2C) showed increased inflow kinetics of Gd-DTPA in SU5416 treated tumors compared to controls. Average k^{trans} values during short infusion of the contrast agent were significantly increased 2-fold in response to SU5416 treatment (controls: 0.028 ± 0.004; SU5416: 0.058 ± 0.018; p = 0.026; Fig. 2D). In addition, peak enhancement in tumor tissue normalized by peak enhancement in arterial blood ($C_{max}TU/C_{max}AIF$) was significantly increased in SU5416 treated animals (Fig. 3A, controls: 0.22 ± 0.03; SU5416: 0.35 ± 0.15; p = 0.026). To further estimate total distribution volumes of contrast agent in tumor tissue, areas below concentration time curves were calculated and normalized to arterial input AUC values (AUC_{TU}/AUC_{AIF}). Following short-term SU5416 treatment, normalized AUC values were significantly increased compared to controls (Fig. 3B controls: 0.51 ± 0.1; SU5416: 0.77 ± 0.08; p = 0.041).

According to the model parameters tumor blood flow and vascular volume was increased in treated animals [blood flow (ml/min/100 g tissue): controls: 8.2 ± 0.6; SU5416: 10.1 ± 1.4; blood volume (ml/100 g tissue): controls: 5.9 ± 2.5; SU5416: 12.1 ± 4.9]. Compared to blood flow and vascular volume no increase of the permeability-surface area product could be observed in treated animals [PS (1/min): controls: 1.3 ± 0.4; SU5416: 1.4 ± 0.3].

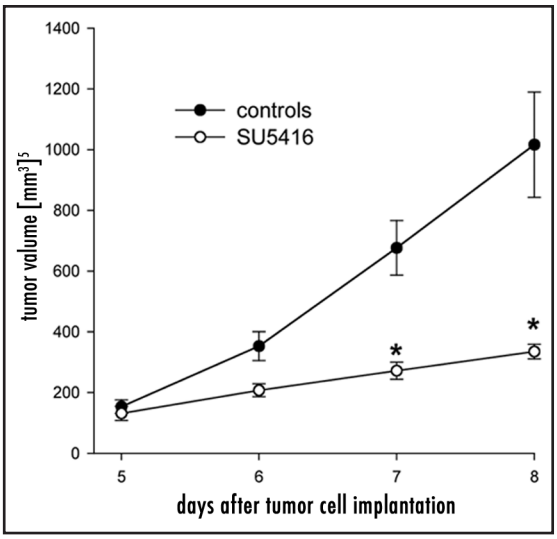

Figure 1. Subcutaneous growth of A-MEL-3 tumors. Animals were treated on day 5, 6 and 7 after tumor cell implantation by i.p. injection of 20 mg/kg SU5416. mean ± SEM; *p < 0.05 vs. controls, Mann-Whitney Rank Sum Test; n = 6 per group.

©2004 LANDES BIOSCIENCE. DO NOT DISTRIBUTE.

In summary, DCE-MRI experiments showed a significantly enhanced initial and overall uptake of Gd-DTPA in SU5416 treated tumors consistent with improved tumor blood flow, blood volume and total distribution space, respectively.

Tumor microcirculation investigated by intravital microscopy. To further elucidate mechanisms responsible for improved blood flow in treated tumors, tumor microcirculation in response to short-term anti-VEGFR treatment was analysed using the dorsal skinfold chamber model combined with intravital fluorescence microscopy. The treatment protocol was identical to CE-MRI experiments in terms of SU5416 dosing and scheduling. Quantitative parameters of tumor microcirculation are summarized in Table 1. Functional vessel density (length of FITC-dextran perfused microvessels related to tumor tissue area) was significantly decreased by 15% in SU5416 treated animals (controls: 206 ± 9 mm^{-1}; SU5416: 175 ± 7 mm^{-1}; p = 0.03). Interestingly however, in treated animals a tendency towards increased tumor vessel diameters, red blood cell velocities and consequently elevated segmental microvascular blood flow was observed. Therefore, a detailed analysis of distribution patterns of tumor vessel diameters and red blood cell velocities was performed. In Figure 4 frequency distributions of microvessel diameters (Fig. 4A) and red blood cell velocities (Fig. 4B) are depicted. In control animals diameters of 973 vessel segments corresponding to an average number of 161 vessel segments per investigated tumor were measured. Analysis of frequency distribution revealed a right skewed (skewness 1.83 ± 0.08) distribution with a calculated kurtosis of 9.76 ± 0.16. SU5416 treatment induced a significant right-shift in the distribution pattern (p < 0.01, Kolomogorov-Smirnov test) towards increased vessel diameters (skewness 1.6 ± 0.10, kurtosis 4.73 ± 0.19). In SU5416 treated animals 650 vessel segments have been analysed corresponding to an average of 130 visible vessel segments analysed in each tumor. The reduced number of vessel segments indicates a less branched microvascular network in treated animals. Representative images illustrating this phenomenon are given in

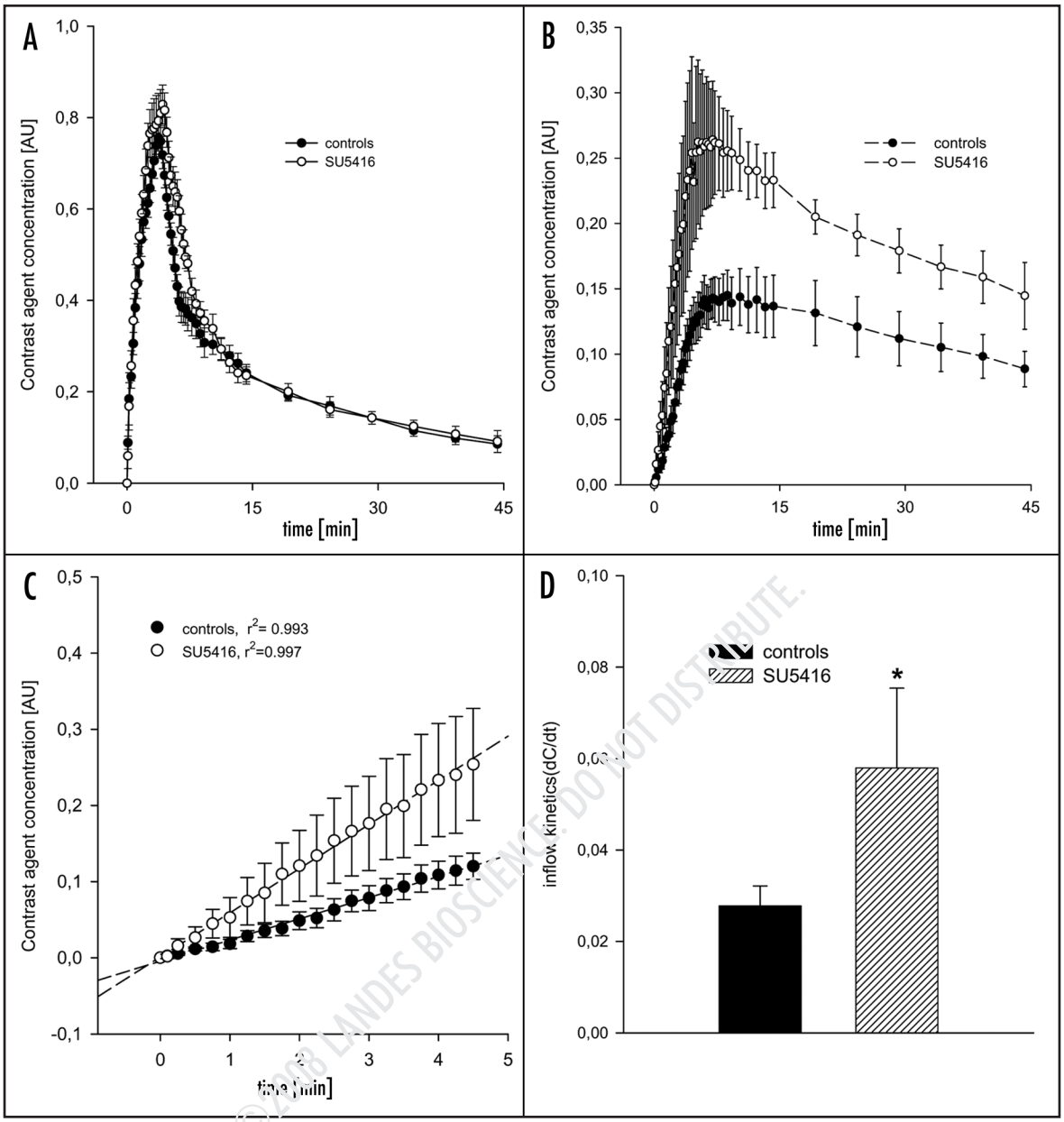

©2008 LANDES BIOSCIENCE. DO NOT DISTRIBUTE.

Figure 2. Concentration-time data quantified by DCE-MRI imaging using the Snapshot-FLASH technique. Arterial input functions (A) and concentration-time-data in tumor tissue (B) after short infusion of Gd-DTPA. The initial uptake kinetic of Gd-DTPA (ΔC/dt) (C and D) was significantly increased in treated animals. Results in (D) are given as mean ± SEM; *p = 0.026 vs. controls, Mann-Whitney Rank Sum Test; n = 6 per group.

Figure 5, in which a less chaotic and less tortuous microvascular network is visible in treated animals (Fig. 5H) compared to controls (Fig. 5G). Analogue to tumor vessel diameters, SU5416 treatment significantly shifted distribution of red blood cell velocities towards faster velocities (Fig. 4B). Skewness and kurtosis were both reduced in response to SU5416 treatment (controls: skewness 3.7 ± 0.12; kurtosis 23.1 ± 0.2; SU5416: skewness 2.7 ± 0.12; kurtosis 10.4 ± 0.3).

Tumor tissue oxygenation. To investigate the effects on tumor oxygen supply, tumor tissue pO_2 values were measured by phosphorescence quenching technique (Fig. 4C). Untreated tumors were hypoxic (mean pO_2:12.9 ± 1.9 mmHg) with a trend towards higher levels in tumor periphery compared to tumor center (periphery 13.9 ± 1.9; center: 11.9 ± 2.2) In treated animals a tendency towards increased pO_2 values (mean pO_2: 16.4 ± 3.7 mmHg) were observed, however a level of significance in terms of changes in pO_2 distribution or mean values in tumor center (12.5 ± 3.3 mmHg) or tumor periphery (20.4 ± 4.3 mmHg) was failed.

Histology. To observe tumor cell viability and necrotic regions H&E staining was performed. An increase in necrotic areas in response to SU5416 therapy (Fig. 5A and B) compared to controls was not observed. In both groups small necrotic areas and hemorrhage could be found, which is typically for these fast growing tumors (Fig. 5C and D). Analysis of tumor microvessels by vWF staining displayed a reduced microvessel density in treated animals compared to controls (Fig. 5E and F). In control tumors a large number of very thin microvessels can be observed, which are almost eliminated in treated tumors. In these tumors remaining vessels display a more

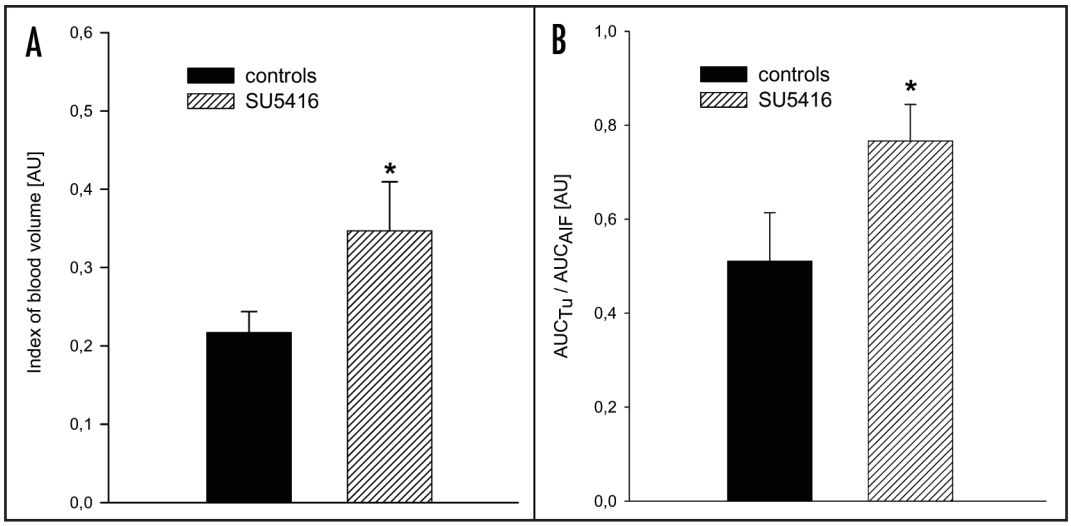

Figure 3. Maximal peak enhancement in tumor tissue normalized to the maximal concentration in arterial blood as index of tumor blood volume (Fig. 3A). Overall uptake of Gd-DTPA in tumor tissue was quantified by calculation of area below concentration-time curve (AUC) values in tumor tissue normalized to the AUC value of the individual arterial input function. Results are given as mean ± SEM; *p = 0.041 vs. controls, Mann-Whitney Rank Sum Test; n = 6 per group.

prominent staining and increased vessel diameters. This finding is consistent with data obtained by intravital microscopy.

Discussion

The data presented here provide further evidence in support of the normalization hypothesis formulated by R. Jain [3,4] Short-term treatment of highly vascularized melanomas by a small molecule kinase inhibitor which blocks phosphorylation of c-kit, FLT3, VEGFR-1, VEGFR-2 (KDR) and VEGFR-3 resulted in an improved microcirculation of tumors quantified by non-invasive CE-MRI. Analysis of tumor microcirculation revealed a reduction of functional vessel density upon therapy as already shown by Vajkoczy et al.[26] and Pahernik et al.[27] However, distribution pattern of vessel diameters and red blood cell velocity were shifted towards increased diameters and faster flow velocities in remaining tumor vessels. Moreover, a less branched microvascular network was identified in treated tumors.

Interestingly, this morphological change was associated with increased inflow kinetics of GD-DTPA, increased peak enhancement and overall uptake of the contrast agent in tumor tissue. The tissue concentration depends on three independent physiological parameters: (1) tumor blood flow, (2) tumor vascular volume and (3) vascular permeability. An increase in overall tissue contrast agent concentration could therefore be explained by increased microvascular permeability, which would be in the opposite of the normalization hypothesis. This effect, however, is of pathophysiological relevance only, if the contrast agent exchange between blood and interstitium is limited by vessel permeability and not by the tissue perfusion or vascular volume. Tumor microvessels are characterized by endothelial fenestration and endothelial gaps and therefore are in general highly permeable for small molecules.[28] Hence, the exchange of small molecular GD-DTPA in tumors is unlikely limited by vascular permeability. In addition to the interstitial perivascular space rapid exchange of the contrast agent in tumors can occur due to large necrotic areas or vascular like structures (vascular mimicry).[29] Histologic examination of tumor tissue did not reveal an increase in necrotic tumor tissue in response to therapy. Therefore, rapid uptake of the contrast agent in necrotic areas can be ruled out to explain increased uptake kinetics of Gd-DTPA. On the other hand increased initial inflow kinetics of the contrast agent and increased peak enhancement indicate increased blood flow and tumor vascular volume. This conclusion is confirmed by tracer-kinetic modelling of concentration time data, which shows an increase of blood perfusion by 19% and a two-fold increase of tumor vascular volume in treated animals. In contrast the permeability-surface area product remained unchanged. Therefore a more conductive tumor microcirculation by increased blood flow and vascular volume in response to therapy can be proposed to be responsible for the increased overall uptake in tumor tissue. Furthermore, this conclusion is in agreement with intravital microscopic data showing a shift towards faster red blood cell velocities and increased vessel diameters.

Analysing microcirculatory changes upon SU5416 therapy in gliomas, Vajkoczy et al. found increased red blood cell velocities and increased blood flow in remnant microvessels[26] as quantified in the present investigation. The authors concluded, that the observed increase of red blood cell velocity did not suffice to efficiently compensate for the reduced vascular density due to a decrease of

Table 1 **Quantitative analysis of tumor microcirculation by intravital microscopy**

	Controls n = 6	SU5416 n = 5
diameter [µm]	12.5 ± 0.7	14.4 ± 1.0
v_{RBC} [µm/s]	95.3 ± 16.2	175.2 ± 45.4
Q [pl/s]	7.5 ± 1.6	18.4 ± 5.6
fvd [1/mm]	206.2 ± 8.8	175.0 ± 6.9*
tissue pO_2 [mmHg]	12.9 ± 1.9	16.4 ± 3.7

Vessel diameters, mean red blood cell velocity (RBC) and functional vessel density (fvd = length of FITC-perfused microvessel related to tumor tissue area) have been measured offline by digital video analysis. Blood flow in vessel segments (Q) was calculated. Tumor tissue pO_2 was measured by phosphorescence quenching technique. *p = 0.03 vs. controls, Mann-Whitney Rank Sum Test; controls: n = 6; SU5416: n = 5.

©LANDES BIOSCIENCE. DO NOT DISTRIBUTE.

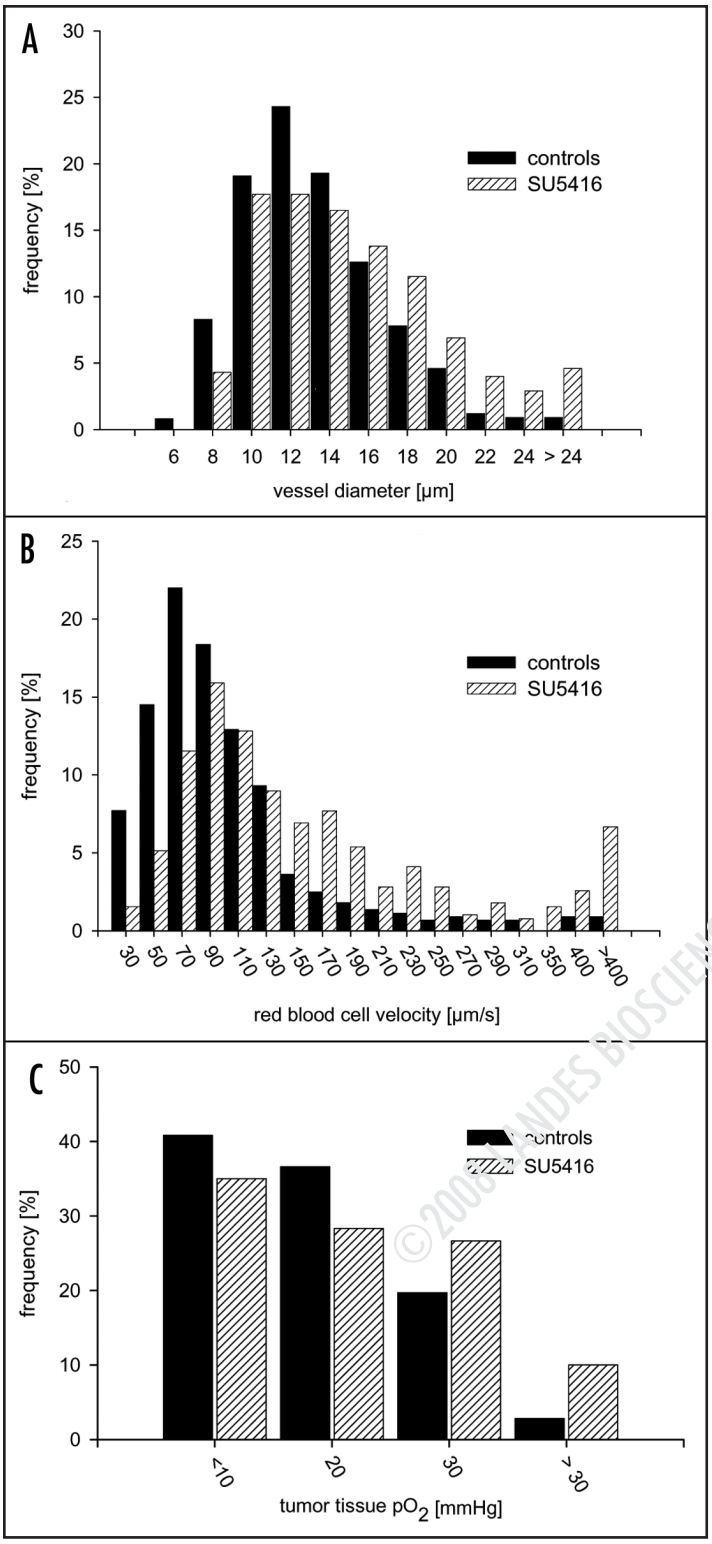

Figure 4. Frequency distributions of vessel diameters (A), red blood cell velocities (B) and tumor tissue oxygenation (C). Frequency distributions have been tested for statistically significant differences using the Kolmogorov-Smirnov test. In response to SU5416 treatment distribution pattern of vessel diameters and red blood cell velocities were significantly shifted towards increased vessel diameters and faster red blood cell velocities. A trend towards elevated tumor tissue pO_2 values was observed.

vascular surface area and an increase of intervascular spacing.[26] Given the fact that increased segmental blood flows could not compensate reduced vascular density, one has to assume decreased oxygen supply to tumor tissue leading to decreased tumor tissue pO_2 values. However, using non-invasive phosphorescence quenching technique, we did not observe decreased tumor tissue pO_2 values in treated animals. In contrast, a trend towards elevated tumor tissue oxygenation upon anti-VEGF treatment was found in the present investigation.

Tumor perfusion and nutritional supply to tumor cells rely on the morphology, vessel diameter and three-dimensional architecture of the vascular network[30] as well as tumor microvessel functionality and vessel maturation. Especially flow in immature vessel segments is chaotic, with intermittent stagnation followed by high-flow or even flow reversal in isolated segments.[31] Consequently overall perfusion is critically determined by the proportion of immature and mature vessels. Therefore, a reduction of microvessel density does not necessarily implicate reduced tumor blood flow. Pruning immature tumor blood vessels with oscillating blood flow as well as hyperperfusion in remaining blood vessels and reduced intratumoral shunt-perfusion may explain a more conductive tumor microvascular network in response to anti-VEGF therapy.

In addition, time of treatment start as well as angiogenic tumor activity need to be critically taken into consideration as factors determining overall functional changes of tumor microcirculation upon anti-VEGF therapy. In order to achieve most effective antitumoral efficacy by an anti-angiogenic agent, in a large number of studies published, anti-angiogenic treatment is started simultaneously or shortly after tumor cell implantation.[26,27,32,33] At this time a functional vascular network is not established in experimental tumors and inhibition of VEGF-signalling effectively prevents sprout formation and the development of a conductive microcirculatory network. In this scenario, treatment critically impedes development of a functional tumor microcirculation, and therefore, significantly deteriorates nutritional supply to tumor cells. However, this scenario is not comparable to the clinical situation, in which advanced tumors with already established vascular networks are presently treated by anti-VEGF therapy combined by chemotherapy.[34] In order to better simulate the clinical situation, in the present investigation a tumor model was chosen, in which an established functional tumor microcirculation comprising both, mature vessels segments and vascular sprouts, is established when treatment was started. Moreover, A-MEL-3 melanomas are characterized by a high angiogenic activity resulting in rapid vessel growth and a rather high percentage of immature vessel segments. Therefore, inhibiting VEGF signalling in this tumor model might induce a relatively strong shift in the balance between mature and immature vessel segments. In contrast, in slow growing tumors with low angiogenic activity, less sprout formation and a high percentage of mature vessel segments, anti VEGF therapy may not induce a more conductive vascular network at all, as the balance between mature and immature vessel segments might not be significantly shifted in response to therapy. For instance, investigating functional tumor blood flow by ultrasound imaging in a slow growing melanoma xenograft model, Cheung et al. recently observed reduced functional tumor blood flow 24 h and 48 h after DC101 treatment.[35] Moreover, long term DC101 treatment over three weeks significantly reduced functional tumor blood flow and tumor volumes in MeWo xenografts.[35] However, compared to tumor

©2008 LANDES BIOSCIENCE. DO NOT DISTRIBUTE

volumes in the present study, Cheung et al. observed grafts with more than 10-fold smaller tumor volumes (up to 25 mm^3).

Due to controversial results published by different research groups, the effects of anti-VEGF treatment on tumor microvascular function observed in our study have to be restricted to the applied tumor model and treatment schedule.

Nevertheless, in accordance with our results a rising number of experimental studies[12,13,36-38] and clinical results[6] support the "normalization" hypothesis envisioned by Rakesh Jain.[3] Further investigations, however, need to systematically clarify, which type of tumors are sensitive to a possible "normalization" process, which treatment schedules have to be applied and how a possible window of tumor microvessel "normalization" can be predicted and monitored. These questions need to be resolved in order to further enhance efficacy of antiangiogenic tumor treatment in combination with chemo- or radiation therapy. In brain tumors for instance, vessel normalization upon antiangiogenic treatment has recently been shown to restore the blood-brain barrier.[37] Chemodistribution to brain tumor cells can therefore be hampered by antiangiogenic drugs.

In conclusion, our results provide further evidence that anti-VEGF therapy in certain tumor types can effectively improve microvascular function leading to improved intratumoral delivery of small molecules. In addition to structural changes of tumor microvessels due to pericyte recruitment in response to VEGF deprivation,[13] a simple shift of the ratio between mature and immature tumor vessels within the microvascular network may effectively result in a more conductive microvascular architecture. This mechanism of action should be critically taken into consideration for further optimization of the timing of antiangiogenic tumor therapy when combined with cytotoxic chemotherapy or radiation.

Material and Methods

Subcutaneous A-MEL-3 tumor model. Following approval by the local ethics committee, all experiments were performed in accordance with the 'UKCCCR' Guidelines for the welfare of animals in experimental neoplasia on male Syrian golden hamsters (40–60g b.w.). All surgical procedures were performed under anaesthesia with ketamine (100 mg/kg b.w. i.p., Ketavet®; Parke-Davis, Berlin, Germany) and xylazine (10 mg/kg b.w. i.p., Rompun®; Bayer, Leverkusen, Germany). Tumor cells (~5 x 10^6) of the amelanotic hamster melanoma A-MEL-3 were implanted subcutaneously into the right flank near the upper foreleg at the level of the heart. Five days after tumor cell implantation, animals were randomly assigned to two experimental groups: animals of the treatment group (n = 6) received an i.p. injection of SU5416 dissolved in DMSO at a dose of 20 mg/kg b.w. on day 5, 6 and 7 after tumor cell transplantation. Animals of the control group (n = 6) received DMSO with equivalent volume and timing. The longer (l) and shorter (w) perpendicular axes and the height (h) of each tumor nodule were measured by a caliper and tumor volume (V) was calculated according to the following equation empirically determined by Weis et al.[15]:

$$V = 0.837 \times l \times w \times h \quad (1)$$

CE-MR imaging. To investigate the effects of short term VEGFR2 inhibition on tumor microcirculation of subcutaneous

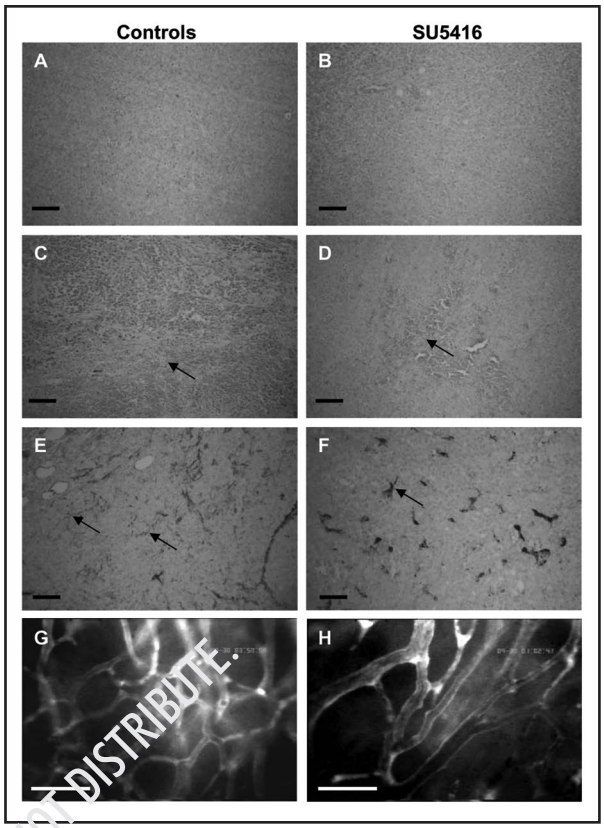

Figure 5. H&E staining of s.c. AMEL-3 tumors of control (A and C) and SU5416 treated animals (B and D). Large areas of vital tumor tissue can be found (A and B) in both groups. Smaller areas of tumor necrosis and hemorrhage (arrows) were observed in control and treated animals. vWF-staining (E and F) displayed a large number of very thin microvessels (arrow) in control tumors (E), which are almost eliminated in treated tumors (F). Intravital microscopy of control tumors (G) displays the typical chaotic tumor vessel architecture. Antiangiogenic treatment (H) induced a less branched and less tortuous microvascular network. Scale bar: 100 µm.

AMEL-3 tumors, DCE-MRI experiments were performed on day eight after tumor cell injection. Prior to MRI investigations, fine polyethylene catheters (Portex Ltd., Hythe, Kent, UK) were inserted into the right jugular vein for infusion of the paramagnetic MR contrast agent. MRI scans was performed on a 9.4 Tesla MR microimaging system with a maximum gradient strength of 200 mT/m and a ^1H birdcage resonator with 38 mm inner diameter as transmit/receive coil (DMX400, Bruker, Karlsruhe, Germany). For MR imaging, hamsters were positioned in an animal handling system, which was then inserted into the resonator with the tumor located in the isocenter of the magnet bore. During the MRI experiment, anesthesia with 1% isoflurane (Abott, Cham, Switzerland) in oxygen was applied at 1.5 l/min via a face mask. ECG and breathing were continuously monitored with an MR compatible physiological animal monitoring unit (Physiogard SM785 NMR, Bruker, Karlsruhe, Germany). To prevent a drop in body temperature during the MRI experiment, the temperature inside the animal handling system was kept constant at 28°C with a warm air heating system. The MRI experiment consisted of (a) a scout scan with three orthogonal slices, allowing for exact positioning of the slice for the DCE-MRI scan which had to intersect both, heart and tumor, (b) three pre-contrast T1 scans, and (c) a total of 47 T1 scans acquired

©2008 LANDES BIOSCIENCE. DO NOT DISTRIBUTE.

over 45 minutes after onset of contrast agent infusion: 32 scans with a 15 s interval, then four scans with a 30 s interval, five scans with a one min interval, and six scans with a five min interval. For (c) the contrast agent gadopentetate dimeglumine (Gd-DTPA, MagnevistTM, Schering AG, Berlin, Germany) was infused at 0.125 ml/min over 4 min (i.e., during the first 16 T1 scans) at a dose of 0.1 mmol/kg body weight.

T1 scans were acquired using an inversion recovery snapshot FLASH sequence.[16] After an initial non-selective fast passage adiabatic inversion pulse, 24 snapshot FLASH images are acquired without any delay in between. Acquisition parameters were as follows: Field of View 40 x 40 mm^2; matrix size 128 x 64 zerofilled to 128 x 128, resulting in an in-plane resolution of 313 µm; slice thickness 1.5 mm; bandwidth 120 kHz. The echo-time was 1.660 ms, the repetition-time 2.636 ms, resulting in an acquisition time of 169 ms per T1-weighted image and a total acquisition time of 4.055 sec per T1 scan allowing for sufficiently accurate sampling of the fast relaxation dynamics in contrast enhanced tissue and blood. From the 24 T1-weighted snapshot FLASH images of each scan a T1 map was calculated using a 3-parameter least square fit on a pixel-by-pixel basis as described by Deichmann et al.[17]

Concentration time data and data analysis. To determine the arterial input function, regions of interest (ROIs) were defined in the centre of the left ventricle. For analysis of concentration-time curves in tumor tissue, ROIs were defined over the total visible tumor section. Concentration-time curves C(*t*) for arterial blood and tumor tissue were calculated from changes in T1 relaxation rates [$\Delta R_1(t)$] between pre- and postcontrast measurements according to the following relation:

$$\Delta R_1(t) = \frac{1}{T_{1post}(t)} - \frac{1}{T_{1pre}(t)} = \alpha \cdot C \qquad (2)$$

where T_{1pre} and T_{1post} (*t*) denote the T_1 relaxation time before and after onset of Gd-DTPA infusion, respectively, and α denotes the relaxivity of the contrast agent. The basic assumption of Eq. 2 is the linearity between T_1 relaxation rate and Gd-DTPA concentration which has been verified experimentally in a previous study.[18]

The slope of initial contrast enhancement during infusion of contrast agent ($dC/dt_{[0\text{-}4.5\ min]}$) and the peak enhancement in tumor tissue over peak enhancement in arterial blood (C_{max}TU/C_{max}AIF) have been calculated to quantitatively analyse differences of concentration-time data. Using Sigmaplot software areas under concentration time courses (AUC) in arterial blood and tumor tissue have been individually calculated for each animal and the quotient between tumor tissue AUC (AUC_{TU}) and the AUC of arterial input function (AUC_{AIF}) is given to indicate total tumor distribution volume of the contrast agent including intravascular and interstitial space (AUC_{TU}/AUC_{AIF}). Concentration-time data were further applied to a tracer-kinetic two-compartment model according to Brix[19,20] to quantify tumor blood flow, tumor vascular volume and the permeability-surface area product.

Dorsal skinfold chamber model and in vivo fluorescence microscopy. To permit quantitative fluorescence analysis of tumor microcirculation, a dorsal skinfold chamber was surgically implanted under general anaesthesia as described in detail elsewhere.[21,22] Implanted tumors were allowed to grow for five days before treatment was started. At this time a well established tumor microvasculature was developed in A-MEL-3 tumors. On day 5, 6 and 7 animals (n = 5) were treated by i.p. injection of 20 mg/kg b.w. SU5416 dissolved in DMSO. Control animals (n = 6) received solvent. Parallel to MRI experiments, investigations by in vivo fluorescence microscopy were performed on day 8.

For intravital microscopy the awake chamber-bearing hamsters were immobilized in a Perspex tube on an individually designed stage (Effenberger, Munich, Germany) under a modified Leitz microscope (Orthoplan; Leitz, Munich, Germany). FITC-labelled dextran (MW 500.000; Sigma, Deisenhofen, Germany) was injected intravenously to visualize tumor microcirculation. Selective observation of FITC-labelled plasma was possible using epiilumination with a 100 W mercury lamp attached to a Ploemopack illuminator with a Leitz 12/3 filter block (excitation 450–490 nm, emission ≥515 nm). In vivo fluorescence microscopy was performed on day 8. In each animal, eight ROIs have been randomly selected. Images were acquired by a CCD camera (Sony, XC-77CE, Sony, Germany) and recorded on S-VHS video tape for subsequent offline analysis.

Analysis of microcirculatory parameters was performed by an image analysis system (Cap Image; Zeintl, Heidelberg, Germany); this system allows the measurement of functional vessel density (fvd), vessel diameter (d) and red blood cell velocity (V_{RBC}). Blood flow in vessel segments (Q) was calculated according to the following equation described by Baker and Wayland:[23]

$$Q = \frac{v_{RBC}}{1.6} \times \left(\frac{d}{2}\right)^2 \times \pi \qquad (3)$$

pO_2 measurements by phosphorescence quenching. In a different set of experiments tumor tissue pO_2 has been non-invasively measured using phosphorescence quenching technique as described in detail earlier.[24] Albumin-bound palladium mesotetra (4-carboxyphenyl) porphyrin (15 mg/kg; Harvard Apparatus, Holliston, MA), was injected i.v.. Following an equilibration period of 10 minutes allowing extravasation of albumin-bound palladium into the tumor interstitial space phosphorescence life time measurements have been performed in 10 ROIs per animal using a 20 X objective. The phosphorescence signal of the tissue resulting from a xenon-flashlamp (Perkin-Elmer, Wiesbaden, Germany; X-strobe, 40 Hz, excitation 540 nm) was detected at ≥590 nm using a photomultiplier tube (P30A-11; Electron Tubes, Middx, UK) and averaged by a digital storage oscilloscope (Tektronix TDS1012; Tektronix Inc., Berkshire, UK). Sixty-four decay signals were averaged to increase the signal-to-noise ratio and the averaged signal was transferred to a computer for analysis of decay time and calculation of pO_2 values. Stored data were fitted to Eq. 4 using the Marquardt-Levenberg method:

$$I_{(t)} = I_{max} \times e^{-t/\tau} + B \qquad (4)$$

where equation 4 is a monoexponential decay, with $I_{(t)}$ is the phosphorescence intensity at time t, I_{max} the maximal phosphorescence intensity, τ the decay time and B the photomultiplier baseline current. pO_2 values were calculated according to:

$$pO_2 = \frac{1}{k_q}\left(\frac{1}{\tau} - \frac{1}{\tau_0}\right) \qquad (5)$$

©LANDES BIOSCIENCE. DO NOT DISTRIBUTE

where k_q = 334 $mmHg^{-1}s^{-1}$ represents the quenching constant at ph 7.4 and 33°C and τ_0 = 657 µs the phosphorescence life time at zero oxygen.[25]

Histology. After MRI experiments have been performed tumors have been harvested and applied to further histological analysis. Tissue samples have been fixed in 4% paraformaldehyd and embedded in paraffin. Sections of tumor tissue with a thickness of 5 µm were taken from all samples. For morphological investigations H&E staining was performed. Tumor blood vessels were visualized by immunostaining with a polyclonal antibody against human von-Willebrand-factor (Dako, Glostrup, Denmark). Sections were incubated for 45 min with the primary antibody diluted 1:200 in PBS-Tween and subsequently developed using the vectastain ABC-Elite-Kit (Vector Laboratories Inc., Burlingame, CA).

Statistical analysis. Results are given as mean ± standard error of the mean (SEM). Statistical analysis of the data was performed using the non-parametric Mann-Whitney test. (Sigmastat; SPSS Inc., Chicago, IL). To describe frequency distributions skewness and kurtosis were calculated using SPSS software (SPSS Inc., Chicago, IL). Differences of frequency distributions of vessel diameters and red blood cell velocities were tested using Kolmogorov-Smirnov test. p values less than 0.05 were considered significant.

Acknowledgements

SU5416 was generously provided by Sugen, Inc. This study was supported by the FöFoLe Research Program, University of Munich, grant Nr. 379.

References

1. Folkman J. Tumor angiogenesis: therapeutic implications. N Engl J Med 1971; 285:1182-6.
2. Folkman J. Role of angiogenesis in tumor growth and metastasis. Semin Oncol 2002; 29:15-8.
3. Jain RK. Normalizing tumor vasculature with anti-angiogenic therapy: a new paradigm for combination therapy. Nat Med 2001; 7:987-9.
4. Jain RK. Normalization of tumor vasculature: an emerging concept in antiangiogenic therapy. Science 2005; 307:58-62.
5. Webb T. Vascular normalization: study examines how antiangiogenesis therapies work. J Natl Cancer Inst 2005; 97:336-7.
6. Batchelor TT, Sorensen AG, di TE, Zhang WT, Duda DG, Cohen KS, Kozak KR, Cahill DP, Chen PJ, Zhu M, Ancukiewicz M, Mrugala MM, Plotkin S, Drappatz J, Louis DN, Ivy P, Scadden DT, Benner T, Loeffler JS, Wen PY and Jain RK. AZD2171, a pan-VEGF receptor tyrosine kinase inhibitor, normalizes tumor vasculature and alleviates edema in glioblastoma patients. Cancer Cell 2007; 11:83-95.
7. Fukumura D and Jain RK. Tumor microvasculature and microenvironment: Targets for anti-angiogenesis and normalization. Microvasc Res 2007; 74:72-84.
8. Brazelle WD, Shi W and Siemann DW. VEGF-associated tyrosine kinase inhibition increases the tumor response to single and fractionated dose radiotherapy. Int J Radiat Oncol Biol Phys 2006; 65:836-41.
9. Klement G, Baruchel S, Rak J, Man S, Clark K, Hicklin DJ, Bohlen P and Kerbel RS. Continuous low-dose therapy with vinblastine and VEGF receptor-2 antibody induces sustained tumor regression without overt toxicity. J Clin Invest 2000; 105:15-24.
10. Kozin SV, Boucher Y, Hicklin DJ, Bohlen P, Jain RK and Suit HD. Vascular endothelial growth factor receptor-2-blocking antibody potentiates radiation-induced long-term control of human tumor xenografts. Cancer Res 2001; 61:39-44.
11. Nieder C, Wiedenmann N, Andratschke N and Molls M. Current status of angiogenesis inhibitors combined with radiation therapy. Cancer Treat Rev 2006; 32:348-64.
12. Tong RT, Boucher Y, Kozin SV, Winkler F, Hicklin DJ and Jain RK. Vascular normalization by vascular endothelial growth factor receptor 2 blockade induces a pressure gradient across the vasculature and improves drug penetration in tumors. Cancer Res 2004; 64:3731-6.
13. Winkler F, Kozin SV, Tong RT, Chae SS, Booth MF, Garkavtsev I, Xu L, Hicklin DJ, Fukumura D, di TE, Munn LL and Jain RK. Kinetics of vascular normalization by VEGFR2 blockade governs brain tumor response to radiation: role of oxygenation, angiopoietin-1 and matrix metalloproteinases. Cancer Cell 2004; 6:553-63.
14. Lin MI and Sessa WC. Antiangiogenic therapy: creating a unique "window" of opportunity. Cancer Cell 2004; 6:529-31.
15. Weiss N, Delius M, Gambihler S, Dirschedl P, Goetz A and Brendel W. Influence of the shock wave application mode on the growth of A-Mel 3 and SSK2 tumors in vivo. Ultrasound Med Biol 1990; 16:595-605.
16. Haase A. Snapshot FLASH MRI. Applications to T1, T2 and chemical-shift imaging. Magn Reson Med 1990; 13:77-89.
17. Deichmann R. and Haase A. Quantification of T1 values by Snaptshot-FLASH NMR imaging. J Magn Reson 1992; 96:608-612
18. Pahernik S, Griebel J, Botzlar A, Gneiting T, Brandl M, Dellian M and Goetz AE. Quantitative imaging of tumor blood flow by contrast-enhanced magnetic resonance imaging. Br J Cancer 2001; 85:1655-63.
19. Brix G, Kiessling F, Lucht R, Darai S, Wasser K, Delorme S and Griebel J. Microcirculation and microvasculature in breast tumors: pharmacokinetic analysis of dynamic MR image series. Magn Reson Med 2004; 52:420-9.
20. Eichhorn ME, Becker S, Strieth S, Werner A, Sauer B, Teifel M, Ruhstorfer H, Michaelis U, Griebel J, Brix G, Jauch KW and Dellian M. Paclitaxel Encapsulated in Cationic Lipid Complexes (MBT-0206) Impairs Functional Tumor Vascular Properties as Detected by Dynamic Contrast Enhanced Magnetic Resonance Imaging. Cancer Biol Ther 2006; 5:89-96.
21. Asaishi K, Endrich B, Götz A and Messmer K. Quantitative analysis of microvascular structure and function in the amelanotic melanoma A-Mel-3. Cancer Res 1981; 41:1898-904.
22. Strieth S, Eichhorn ME, Sauer B, Schulze B, Teifel M, Michaelis U and Dellian M. Neovascular targeting chemotherapy: encapsulation of paclitaxel in cationic liposomes impairs functional tumor microvasculature. Int J Cancer 2004; 110:117-24.
23. Baker M and Wayland H. On-line volume flow rate and velocity profile measurement for blood in microvessels. Microvasc Res 1974; 7:131-43.
24. Helmlinger G, Yuan F, Dellian M and Jain RK. Interstitial pH and pO_2 gradients in solid tumors in vivo: high-resolution measurements reveal a lack of correlation. Nat Med 1997; 3:177-82.
25. Lo LW, Koch CJ and Wilson DF. Calibration of oxygen-dependent quenching of the phosphorescence of Pd-meso-tetra (4-carboxyphenyl) porphine: a phosphor with general application for measuring oxygen concentration in biological systems. Anal Biochem 1996; 236:153-60.
26. Vajkoczy P, Menger MD, Vollmar B, Schilling L, Schmiedek P, Hirth KP, Ullrich A and Fong TA. Inhibition of tumor growth, angiogenesis and microcirculation by the novel Flk-1 inhibitor SU5416 as assessed by intravital multi-fluorescence videomicroscopy. Neoplasia 1999; 1:31-41.
27. Pahernik S, Harris AG, Schmitt-Sody M, Krasnici S, Goetz AE, Dellian M and Messmer K. Orthogonal polarisation spectral imaging as a new tool for the assessment of antivascular tumor treatment in vivo: a validation study. Br J Cancer 2002; 86:1622-7.
28. Dvorak HF, Nagy JA and Dvorak AM. Structure of solid tumors and their vasculature: implications for therapy with monoclonal antibodies. Cancer Cells 1991; 3:77-85.
29. Folberg R, Hendrix MJ and Maniotis AJ. Vasculogenic mimicry and tumor angiogenesis. Am J Pathol 2000; 156:361-81.
30. Konerding MA, Miodonski AJ and Lametschwandtner A. Microvascular corrosion casting in the study of tumor vascularity: a review. Scanning Microsc 1995; 9:1233-43.
31. Munn LL. Aberrant vascular architecture in tumors and its importance in drug-based therapies. Drug Discov Today 2003; 8:396-403.
32. Buerkle MA, Pahernik SA, Sutter A, Jonczyk A, Messmer K and Dellian M. Inhibition of the alpha-nu integrins with a cyclic RGD peptide impairs angiogenesis, growth and metastasis of solid tumors in vivo. Br J Cancer 2002; 86:788-95.
33. Fong TA, Shawver LK, Sun L, Tang C, App H, Powell TJ, Kim YH, Schreck R, Wang X, Risau W, Ullrich A, Hirth KP and McMahon G. SU5416 is a potent and selective inhibitor of the vascular endothelial growth factor receptor (Flk-1/KDR) that inhibits tyrosine kinase catalysis, tumor vascularization and growth of multiple tumor types. Cancer Res 1999; 59:99-106.
34. Eichhorn ME, Kleespies A, Angele MK, Jauch KW and Bruns CJ. Angiogenesis in cancer: molecular mechanisms, clinical impact. Langenbecks Arch Surg 2007; 392:371-9.
35. Cheung AM, Brown AS, Cucevic V, Roy M, Needles A, Yang V, Hicklin DJ, Kerbel RS and Foster FS. Detecting vascular changes in tumor xenografts using micro-ultrasound and micro-CT following treatment with VEGFR-2 blocking antibodies. Ultrasound Med Biol 2007; 33:1259-68.
36. Jain RK, Tong RT and Munn LL. Effect of vascular normalization by antiangiogenic therapy on interstitial hypertension, peritumor edema and lymphatic metastasis: insights from a mathematical model. Cancer Res 2007; 67:2729-35.
37. Claes A, Wesseling P, Jeuken J, Maass C, Heerschap A and Leenders WP. Antiangiogenic compounds interfere with chemotherapy of brain tumors due to vessel normalization. Mol Cancer Ther 2008; 7:71-8.
38. Taguchi E, Nakamura K, Miura T, Shibuya M and Isoe T. Anti-tumor activity and tumor vessel normalization by the vascular endothelial growth factor receptor tyrosine kinase inhibitor KRN951 in a rat peritoneal disseminated tumor model. Cancer Sci 2008; 99:623-30.

©2008 LANDES BIOSCIENCE. DO NOT DISTRIBUTE.